

Strengthening the virtual-source method for time-lapse monitoring

Kurang Mehta¹, Jon L. Sheiman¹, Roel Snieder², and Rodney Calvert³

ABSTRACT

Time-lapse monitoring is a powerful tool for tracking subsurface changes resulting from fluid migration. Conventional time-lapse monitoring can be done by observing differences between two seismic surveys over the surveillance period. Along with the changes in the subsurface, differences in the two seismic surveys are also caused by variations in the near-surface overburden and acquisition discrepancies. The virtual-source method monitors below the time-varying near-surface by redatuming the data down to the subsurface receiver locations. It crosscorrelates the signal that results from surface shooting recorded by subsurface receivers placed below the near-surface. For the Mars field data, redatuming the recorded response down to the permanently placed ocean-bottom cable (OBC) receivers using the virtual-source method allows one to reconstruct a survey as if virtual

sources were buried at the OBC receiver locations and the medium above them were a homogeneous half-space. Separating the recorded wavefields into upgoing and downgoing (up-down) waves before crosscorrelation makes the resultant virtual-source data independent of the time-varying near-surface (seawater). For time-lapse monitoring, varying source signature for the two surveys and for each shot is also undesirable. Deconvolving the prestack crosscorrelated data (correlation gather) by the power spectrum of the source-time function results in virtual-source data independent of the source signature. Incorporating up-down wavefield separation and deconvolution of the correlation gather by the source power spectrum into the virtual-source method suppresses the causes of nonrepeatability in the seawater along with acquisition and source signature discrepancies. This processing combination strengthens the virtual-source method for time-lapse monitoring.

INTRODUCTION

The virtual-source method (Bakulin and Calvert, 2004, 2006) images and monitors below a complex overburden without knowledge of overburden velocities and near-surface changes. The virtual-source method is closely related to seismic interferometry (Claerbout, 1968; Derode et al., 2003; Schuster et al., 2004; Snieder, 2004; Wapenaar, 2004; Bakulin and Calvert, 2005; Wapenaar et al., 2005; Curtis et al., 2006; Korneev and Bakulin, 2006; Larose et al., 2006; Snieder et al., 2006b). Seismic interferometry states that crosscorrelating the recording of a given pair of receivers when summed over the physical sources results in an impulse response between the two receivers. Apart from imaging below a complex overburden, the virtual-source method is proposed for time-lapse monitoring, provided the receivers are placed permanently below the time-varying overburden.

Time-lapse monitoring is a powerful tool for tracking changes in the subsurface (Rickett and Claerbout, 1999; Koster et al., 2000; Lumley, 2001; Kragh and Christie, 2002; Calvert, 2005; Naess, 2006). These changes include geomechanical phenomena associated with fluid migration. Conventionally, the changes associated with fluid migration can be tracked by observing the differences between two seismic surveys obtained over the surveillance period. Differences between the two surveys also include (1) changes resulting from geomechanical effects in the overburden and (2) acquisition discrepancies (Naess, 2006), such as those in the source location and source signature between the base and the monitor survey.

We apply the virtual-source method to ocean-bottom cable (OBC) data acquired at the Mars field in the deepwater Gulf of Mexico (Mehta et al., 2006). Data for the base survey were acquired in October and November 2004; the repeat (monitor) survey was conducted in June 2005. During acquisition, 120 four-component (4-C) sensors were placed permanently (50 m apart) on the seafloor (1 km deep)

Manuscript received by the Editor 20 February 2007; revised manuscript received 2 October 2007; published online 11 April 2008.

¹Shell International E & P, Houston, Texas, U.S.A. E-mail: kurangmehta@gmail.com; jonathan.sheiman@shell.com.

²Colorado School of Mines, Department of Geophysics, Center for Wave Phenomena, Golden, Colorado, U.S.A. E-mail: rsnieder@mines.edu.

³Deceased 22 November 2007.

© 2008 Society of Exploration Geophysicists. All rights reserved.

and 364 air guns were shot every 25 m near the sea surface (Figure 1). A region of 40 missing shots exists because of a platform above receiver 80.

The preprocessing of conventional OBC data includes source depulsing and suppression of the free-surface reflection and multiples using dual sensor summation. The preprocessed seismic data are then migrated using prestack Kirchhoff depth migration to obtain a depth section of the seismic image.

Using the Mars field velocity model, the depth image corresponding to the 2004 data is converted to a time image (Figure 2) for comparison with the images generated by the virtual-source data. The time $t = 0$ denotes the seafloor level. The blanking just below the seafloor level is applied to the image gathers to mute the data having large opening angles at the reflection point. This suppresses the stretching of the source wavelet (NMO stretching) at large opening angles. The mute zone for later times (3–4 s) corresponds to a salt body. The ellipse around 3–4 s highlights the reservoir layers.

In the next section, we discuss the causes of undesirable nonrepeatability between time-lapse surveys for the Mars field OBC data and reasons for using the virtual-source method for time-lapse monitoring. We then compare the images for 2004 and 2005 obtained by migrating virtual-source data and their normalized differences. In the sections to follow, we observe strengthening the virtual-source method by incorporating upgoing-downgoing (up-down) wavefield separation to minimize the influence of time-varying seawater on the

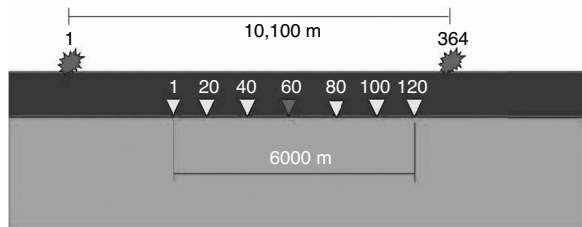


Figure 1. Sketch of the geometry of the Mars field OBC data acquisition, where 120 four-component sensors (triangles) are placed permanently every 50 m on the seafloor; 364 air guns (stars), spaced every 25 m, are fired from the sea surface with a region of 40 missing shots (caused by the presence of the platform) above receiver 80. Water depth is 1 km.

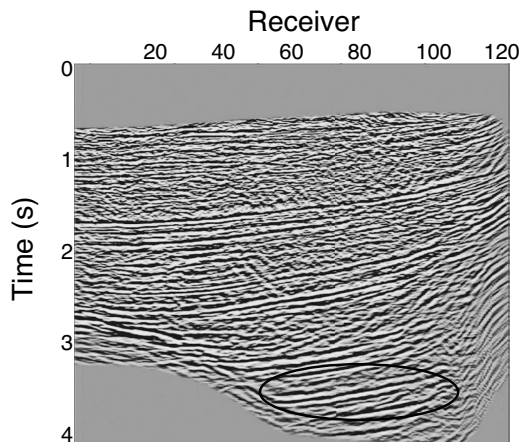


Figure 2. Seismic image generated after migrating conventional OBC data acquired in 2004.

virtual-source data. Finally, we illustrate that deconvolution of the correlation gather by the source power spectrum suppresses the effect of time-varying source power spectrum in the virtual-source data. Combining up-down wavefield separation and deconvolution by the source power spectrum thus strengthens the virtual-source method for time-lapse monitoring.

WHY THE VIRTUAL-SOURCE METHOD?

Often, the discrepancies between two seismic surveys aimed at time-lapse monitoring include not only the changes at the reservoir level but also prominent and undesirable changes in the overburden that mask the changes in the reservoir resulting from fluid migration. For the Mars field, the variations in the seawater include changes in seawater level, sea-surface roughness, seawater temperature, and salinity.

An important advantage of applying the virtual-source method for time-lapse monitoring is the ability to redatum the data down to the permanently placed OBC receivers. The virtual-source gathers are expected to be independent of variations in the seawater as well as acquisition discrepancies (source location and source power spectrum) for the two surveys. The source power spectrum varies not only for the two surveys but also for each shot location.

Let A and B be two receivers. The wavefields excited by a single source recorded by the receivers, are, in the frequency domain, given by

$$\begin{aligned} U(\mathbf{r}_A, \mathbf{r}_S, \omega) &= S(\omega)G(\mathbf{r}_A, \mathbf{r}_S, \omega), \\ U(\mathbf{r}_B, \mathbf{r}_S, \omega) &= S(\omega)G(\mathbf{r}_B, \mathbf{r}_S, \omega), \end{aligned} \quad (1)$$

where $S(\omega)$ is the frequency-domain representation of the source wavelet; $G(\mathbf{r}_A, \mathbf{r}_S, \omega)$ is the Green's function for wave propagation from the source to receiver A ; $G(\mathbf{r}_B, \mathbf{r}_S, \omega)$ is the Green's function for wave propagation from the source to receiver B ; and \mathbf{r}_S , \mathbf{r}_A , and \mathbf{r}_B are the coordinates of the source and the two receivers A and B , respectively.

Crosscorrelating the wavefields recorded by receivers A and B corresponds, in the frequency domain, to

$$\begin{aligned} U(\mathbf{r}_A, \mathbf{r}_S, \omega)U^*(\mathbf{r}_B, \mathbf{r}_S, \omega) &= |S(\omega)|^2G(\mathbf{r}_A, \mathbf{r}_S, \omega) \\ &\quad \times G^*(\mathbf{r}_B, \mathbf{r}_S, \omega), \end{aligned} \quad (2)$$

where the asterisk indicates the complex conjugate. Along with the correlation of the Green's functions, the right-hand side of equation 2 also contains the power spectrum of the source-time function. Note the crosscorrelation is independent of the phase spectrum of the source-time function. The power spectrum of the source pulse may vary for different shots as well as for different surveys. Variations in the source power spectrum can be removed by deconvolving the correlation gather with the power spectrum of the source wavelet (addressed later in this article).

Apart from deconvolution by the power spectrum of the source-time function, the virtual-source method (seismic interferometry) requires a continuous, uniform distribution of sources surrounding the receivers and careful integration over the sources (Wapenaar et al., 2005) with appropriate weights and scaling. A uniform distribution of the sources also provides well-balanced angular illumination of the subsurface. For geophysical applications, however, we cannot have sources all around the downhole receivers. With a limited source aperture, the resulting virtual-source data agree kinematically with the active source data (Mehta et al., 2007c). In the case of any

time-lapse change, the difference in the virtual-source images would only depict the traveltimes changes reliably. Thus, extracting correct amplitudes in the virtual-source method and estimating amplitude (dynamic) differences in time-lapse applications is a topic of future research.

VIRTUAL-SOURCE METHOD

To generate a virtual-source gather, we first correlate the wavefield recorded by a reference receiver (virtual source) with the wavefield recorded by another receiver. The resultant correlation gather when summed over the physical sources gives a trace that corresponds to the recording by the other receiver as if there were a source (virtual source) at the reference receiver location (Bakulin and Calvert, 2004, 2006). For a chosen reference receiver (virtual source), this procedure generates a virtual-source gather when repeated for every other receiver. We generate virtual-source gathers for every receiver acting as a virtual source and migrate the resulting virtual-source gathers in 2004 and 2005 using prestack Kirchhoff depth migration.

To quantify the differences between the time-lapse images, we compute the normalized difference of the two images, defined as

$$\text{Diff} = \frac{M - B}{\text{rms}(B)}, \quad (3)$$

where B represents the base survey (2004) and M represents the monitor survey (2005). We also quantify the repeatability using the normalized root mean square (nrms) of the difference of the images in 2004 and 2005. The nrms (Kragh and Christie, 2002) of the difference is defined as

$$\text{nrms} = \frac{200[\text{rms}(M - B)]}{\text{rms}(M) + \text{rms}(B)}, \quad (4)$$

where the rms operator is defined as

$$\text{rms}(A) = \sqrt{\frac{\sum_1^N A^2}{N}}. \quad (5)$$

In equation 5, N is the number of samples. Although the virtual-source data generated here do not have true amplitudes, nrms is a good measure of the relative amplitudes of the difference and the original virtual-source image. A decrease in the nrms value indicates an improvement in repeatability.

The simplest approach to generate a virtual-source gather is to correlate the total wavefield at the virtual source with the total wavefield at the receivers (Mehta et al., 2006). The virtual-source gather (with receiver 60 as the virtual source) obtained using the simplest approach (Figure 3a) is dominated by a strong reflection around 1.3 s. This strong reflection comes from the sea surface because we correlate the total wavefields at the virtual source and the receivers (Mehta et al., 2007a; Mehta et al., 2007b). We generate similar virtual-source gathers using every receiver as the virtual source.

The images for 2004 and 2005, obtained by migrating the virtual-source data (Figure 3a), are shown in Figure 4a and b, respectively. The same Mars field velocity model is used for migrating both sets of virtual-source data. We convert the resultant depth images to time images for a possible comparison of the images with the virtual-source data and the conventional OBC image. Similar to the virtual-source data (Figure 3a), the virtual-source images are also dominat-

ed by the reflection from the sea surface, labeled as ‘‘Free-surface multiple.’’ Compared to the conventional OBC image (Figure 2), the expected reservoir layers highlighted by the ellipse are imaged poorly.

To differentiate the 2004 and 2005 images, we show the normalized difference image in Figure 4c. The difference is obtained by locally time-aligning the traces to account for any geomechanical

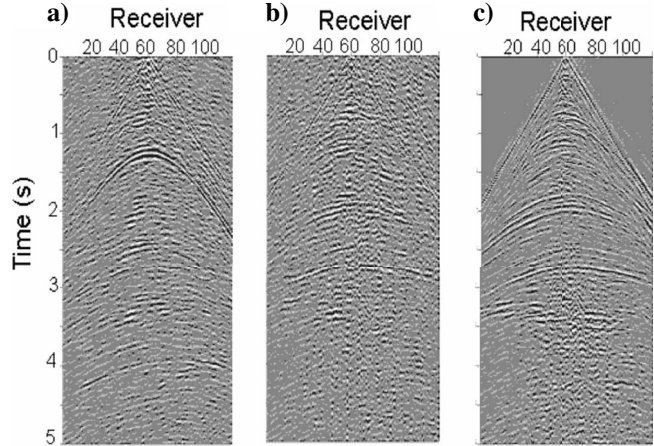


Figure 3. A representative virtual-source gather (with receiver 60 as the virtual source) generated by correlating (a) total wavefields at the virtual source and the receivers, (b) the downgoing waves at the virtual source with the upgoing waves at the receivers, and (c) the direct arrival windowed in the downgoing waves at the virtual source with the upgoing waves at the receivers.

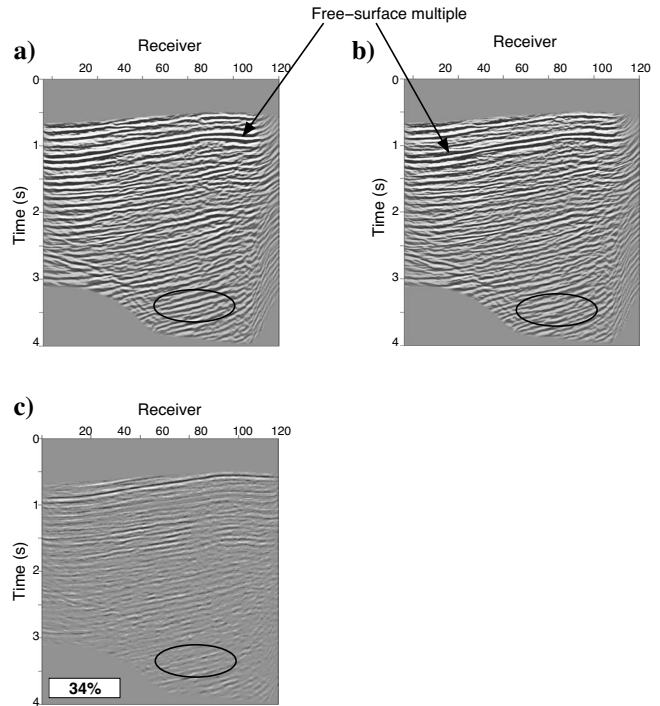


Figure 4. Images generated by migrating the virtual-source data. Virtual-source gathers are generated by correlating the total wavefield at the virtual source with the total wavefield at the receivers. (a) Image for 2004 data. (b) Image for 2005 data. (c) Normalized difference of the two images, after local time alignment. The nrms value is shown in the box on (c).

changes in the subsurface and to separate out the changes within the reservoir from its gross movement. The local time alignment was done by locally correlating traces in small time windows. These time shifts were relatively small (approximately ± 2 ms). To separate changes within the reservoir from its gross movement resulting from geomechanical phenomena in the subsea environment, similar time shifts are also applied to the images displayed in the rest of the article.

At the Mars field, no production-related subsurface changes were observed within the reservoir over the surveillance period (between the base and the monitor survey). The nrms should, ideally, be zero. Although there were no observable production-related changes at the Mars field, for the virtual-source data generated by correlating total wavefields, the normalized difference image (Figure 4c) shows significant and coherent events. The nrms value of the difference of the virtual-source images generated by correlating total wavefield is 34%. This nonzero nrms value can be attributed to variations in the seawater properties and acquisition discrepancies.

Table 1 lists the nrms of the difference for the virtual-source images obtained by using different combinations of wavefields for correlation. The last four columns indicate the causes of nonrepeatability. For each virtual-source image (i.e., for each row in the table), the plus or minus sign indicates the presence or suppression of variations from the corresponding cause of nonrepeatability.

For the virtual-source data generated by correlating the total wavefields, the first row in Table 1 lists the causes of the undesirable time-lapse discrepancies (Figure 4c). The discrepancies are mainly caused by variations in the seawater. We correlate total wavefields; therefore, after being redatumed at the seafloor, the waves excited by the virtual source propagate not only through the subsurface (solid rays in Figure 5a) but also through the seawater (dashed rays in Figure 5a).

Waves propagating along the dashed rays are influenced by the time-lapse variation in the seawater: variations in water level, sea-surface roughness, water temperature, and salinity. In terms of acquisition discrepancies, the variation in the location of the source is removed because the virtual-source method redatums the OBC data by creating virtual sources at each permanently placed seafloor re-

ceiver location. The variation attributable to the source power spectrum (equation 2), however, still exists. These variations in the seawater and source signature discrepancies contribute to the prominent undesirable differences observed in Figure 4c and the nonzero nrms value.

WAVEFIELD SEPARATION

The reflections from the sea surface (dashed rays in Figure 5a) are sensed by the OBC receivers mainly as downgoing waves. If, instead of correlating the total wavefields, the downgoing waves at the virtual source are correlated with the upgoing waves at the receivers, the free-surface multiple (along with other downgoing reflections sensed by the receivers) can be suppressed (Mehta et al., 2007a). Snieder et al. (2006a) show that in structural engineering, the reflections from the base off a building can be eliminated by conducting seismic interferometry using upgoing waves that create a virtual source at a reflectionless interface.

To make the virtual-source data independent of the seawater variations, we follow the approach by Mehta et al. (2007a). Instead of correlating total wavefields, we generate virtual-source gathers by correlating the downgoing waves at the virtual source with the upgoing waves at the receivers. For OBC data, up-down wavefield separation of the wavefield is possible by dual-sensor summation (e.g., Robinson, 1999).

Figure 3b, noted earlier, is a representative virtual-source gather (receiver 60 is the virtual source) generated after wavefield separation. Because of wavefield separation, the free-surface multiple is suppressed and reservoir reflections (close to 3 s) are visible. Figure 6a and b are the images for 2004 and 2005, respectively, obtained by migrating all such virtual-source gathers generated after wavefield separation into upgoing and downgoing waves. Migration of the virtual-source data generated by correlating the downgoing waves at the virtual source with the upgoing waves at the receivers images the reservoir highlighted by the ellipse. Figure 6c is the normalized difference of the sections for 2004 and 2005.

The nrms of the difference image after up-down wavefield separation is 26% (Table 1). The decrease in the value of nrms compared to the simplest approach indicates an improvement in repeatability after up-down wavefield separation because the waves propagate predominantly through the subsurface. Up-down wavefield separation applied to the virtual-source method suppresses the downgoing reflections and multiples coming from the seawater, making the virtual-source image less sensitive to the changes in the seawater (solid rays in Figure 5b).

The normalized difference image has some low-amplitude coherent events. These events could be the reflections and multiples that are downgoing at the virtual source, upgoing at the receivers, and propagating through the time-varying water layer (dashed rays in Figure 5c). These reflections and multiples cannot be eliminated even by applying up-down wavefield separation to the virtual-source method.

We can further reduce the undesirable variations in the time-lapse virtual-source data by windowing the direct arrival in the downgoing waves

Table 1. Comparison of the nrms values for different seismic images. Tot: tot — virtual-source data generated by correlating total wavefield at the virtual source with the total wavefield at the receivers. Dir — direct arrival windowed in the total wavefield. Down — downgoing waves. Up — upgoing waves. Down-dir — direct arrival windowed in the downgoing waves. Decon — deconvolution of the correlation gather by the source power spectrum. The corresponding figure number is mentioned in the second column. The nrms values are shown in the third column. The last four columns show the progressive strengthening of the virtual-source method for time-lapse monitoring by suppressing the variations in the source location, seawater, S-waves, and source signature. A plus sign denotes the presence of variation and a minus sign denotes the absence of variation.

Seismic image	Fig no.	nrms	Source location variations	Seawater variations	S-wave variations	Source signature variations
Tot:tot	4	34%	—	+	+	+
Down:up	6	26%	—	—	+	+
Down-dir:up	7	17%	—	—	—	+
Down:up:decon	9	16%	—	—	+	—
Down-dir:up:decon	10	14%	—	—	—	—

at the virtual source instead of using all downgoing waves. By windowing the direct arrival in the downgoing waves and muting the rest of the downgoing waves, we impose a P-wave virtual source and hence prevent it from radiating shear waves.

Figure 3c, noted earlier, shows the virtual-source gather after windowing the direct arrival in the downgoing waves at the virtual source. The reservoir reflections are prominent, and the near-subsea reflections are crisp. The images for 2004 and 2005, obtained by mi-

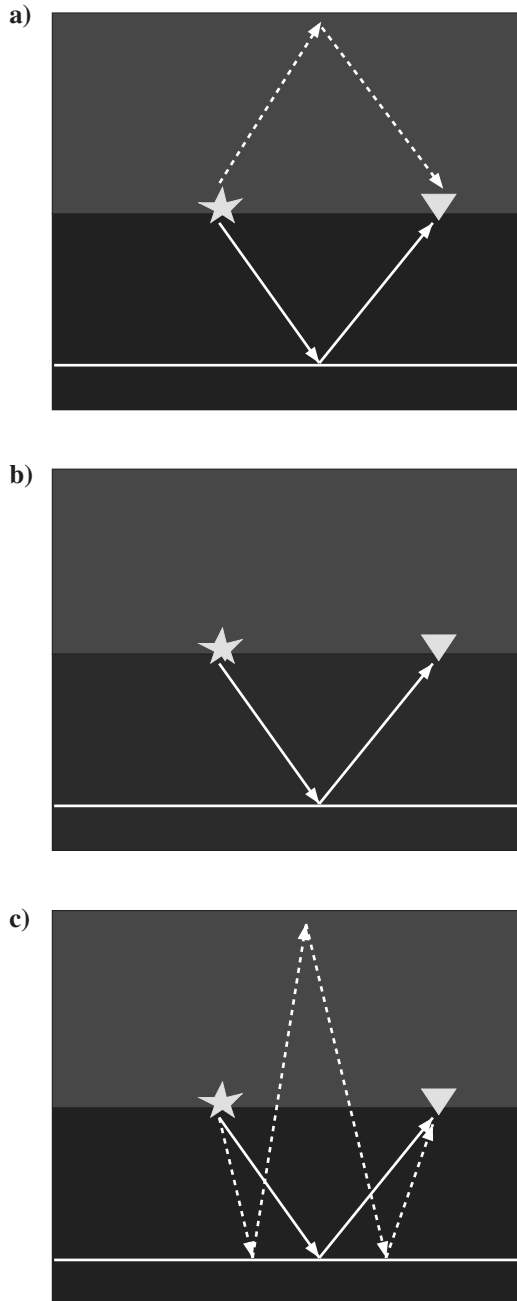


Figure 5. Sketch of the raypaths corresponding to (a) virtual-source data generated by correlating the total wavefield at the virtual source with the total wavefield at the receivers, (b) data generated by correlating the downgoing waves at the virtual source with the upgoing waves at the receivers. (c) Sketch of the raypaths of the multiple that propagates through the overburden even after applying wavefield separation to the virtual-source method.

grating the resulting virtual-source gathers, are shown in Figure 7a and b, respectively. The reservoir layers, highlighted by the ellipse, are well imaged in both sections. Figure 7c is the normalized difference of the images for 2004 and 2005. Compared to using only the up-down wavefield separation, the nrms of the difference image after combining up-down wavefield separation and windowing the direct arrival reduces to 17% (Table 1).

Bakulin and Calvert (2004, 2006) and Mehta et al. (2007a) address the advantage of windowing the direct arrival instead of using all downgoing waves. Figure 7 shows that windowing the direct arrival in the downgoing waves suppresses the nonrepeatability in the shear waves at the virtual source. However, the reflections and multiples that are downgoing at the virtual source, upgoing at the receivers, and propagating through the time-varying water layer (dashed rays in Figure 5c) still exist.

As a result of windowing the direct arrival, we miss the contribution of the P-wave coda to the virtual source. A better approach would be to perform an up-down separation and a P-S separation and then use the downgoing P-waves to create a P-wave virtual source. Similar to amplitude extraction, P-S separation for the virtual-source method is a topic for future research.

Applying up-down wavefield separation to the virtual-source method reduces the nrms values, improving the repeatability. Improvement in the virtual-source method by up-down wavefield separation applied to the Mars field suppresses the variation in the seawater, shear waves, and source location. The variation in the source power spectrum (equation 2), however, still exists in the images gen-

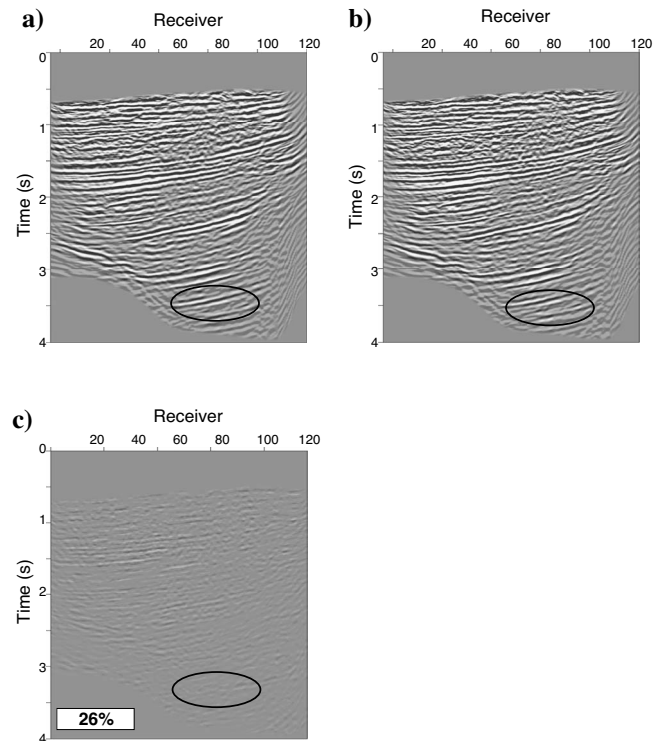


Figure 6. Images generated by migrating the virtual-source data. Virtual-source gathers are generated by correlating the downgoing waves at the virtual source with the upgoing waves at the receivers. (a) Image for 2004 data. (b) Image for 2005 data. (c) Normalized difference of the two images, after local time alignment, showing the nrms value in the box.

erated after applying up-down wavefield separation to the virtual-source method.

SOURCE POWER SPECTRUM VARIATION

The crosscorrelation of the wavefields recorded by a given pair of receivers (equation 2) contains the power spectrum of the source wavelet; thus, the correlation gather must be deconvolved by the source power spectrum (Derode et al., 2003; Schuster et al., 2004; Snieder, 2004; Wapenaar, 2004; Wapenaar et al., 2005). Typically, the source pulse varies not only between the two surveys but also for each shot. Because we use air guns as sources, variation in the source pulse is mainly from changes in the air bubble. In this study, the air-gun ghost is considered part of the air-gun source signature.

The preprocessing applied to conventional OBC data includes source depulsing, which was done as follows. Small-offset traces were taken from each shot; the waves, in a time window of 400 ms around the direct arrival, were aligned. The time window was chosen to include the bubble. These aligned traces were averaged; then filters were derived to turn these responses into band-limited delta functions. The same procedure was applied to both surveys to obtain the same desired band-limited delta function. This conventional preprocessing aimed to remove the variations in the bubble but was not sensitive enough to remove these bubble variations completely.

The source power spectrum corresponds, in the time domain, to the autocorrelation of the source wavelet. This autocorrelation varies because of changes in the residual bubble i.e., part of the air bubble that source depulsing could not suppress. The variation of the au-

tocorrelation of the source pulse (for receiver 90) as a function of source location for the 2004 and 2005 data sets is shown in Figure 8a and b, respectively. Each view is the autocorrelation of the direct arrival windowed in the downgoing waves at receiver 90 for all of the source locations.

Downgoing waves are used for correlation to avoid any near-sea-floor reflection interfering with the autocorrelation of the source pulse. The autocorrelation of the source pulse varies not only between the two surveys but also for each source location. The event close to ± 0.35 s is the residual bubble. Apart from the residual bubble, curved events are present for both causal and acausal times. These curved events correspond to the interference of reflected and refracted waves with the direct arrival for later times and larger off-sets.

Figure 8c is the difference in the autocorrelation of the source pulse for 2004 and 2005. The difference in the main lobe (close to time $t = 0$) is negligible, suggesting that preprocessing adequately equalized the primary source pulses. The curved events also appear to diminish in the difference. The event occurring around ± 0.35 s, however, is the difference in the residual bubble and is pronounced and consistent for every source location. This consistent difference could be from the variation in the water temperature between the two surveys; the base survey was conducted in October and the repeat survey in June. Different sources (air gun) for the two surveys, different air-gun pressures, different depths of source arrays, and discrepancies in sea-surface roughness could also cause the systematic variation in the residual bubble.

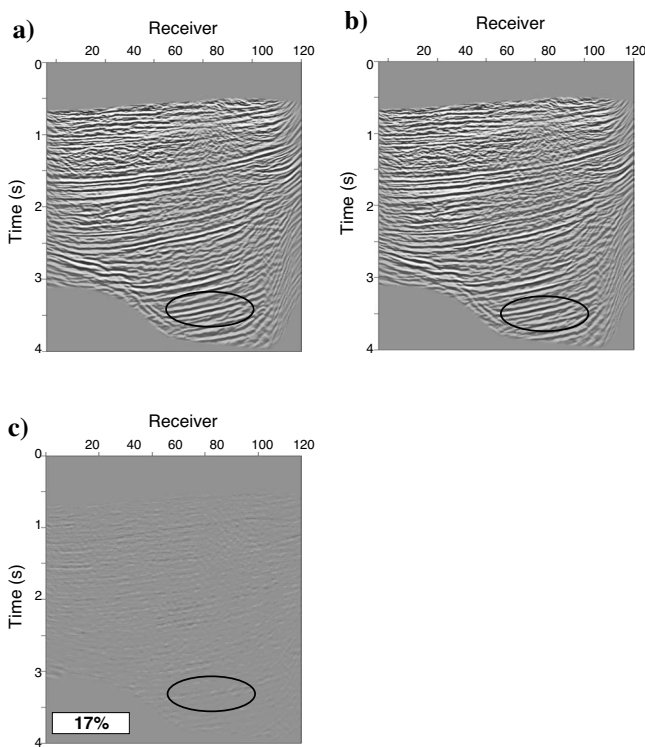


Figure 7. Images generated by migrating the virtual-source data. Virtual-source gathers are generated by correlating the direct arrival windowed in the downgoing waves at the virtual source with the upgoing waves at the receivers. (a) Image for 2004 data. (b) Image for 2005 data. (c) Normalized difference of the two images, after local time alignment, showing the nrms value in the box.

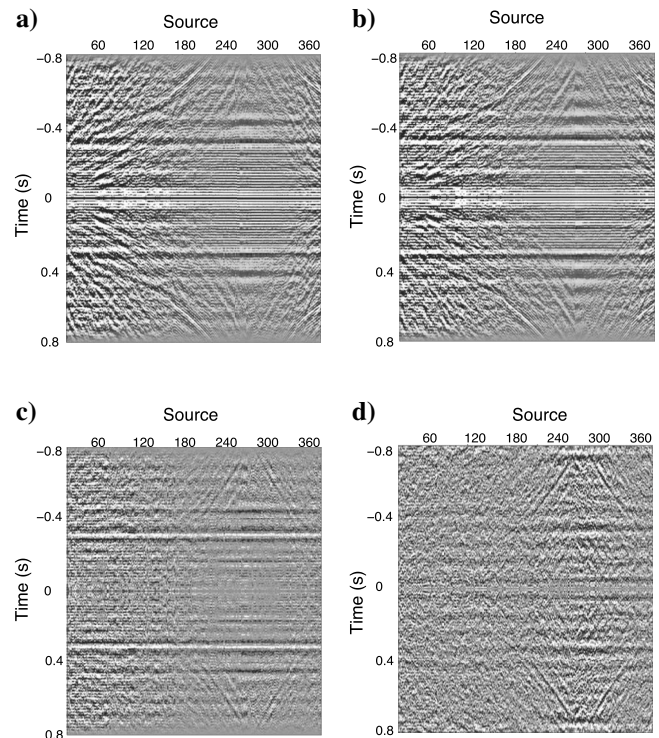


Figure 8. Variation of the autocorrelation of the source pulse corresponding to receiver 90 as a function of source location for (a) 2004 and (b) 2005 data. (c) The difference of the gathers in (a) and (b), obtained on the same scale. (d) Difference of the self-decons (convolution of the source power spectrum and filter that represents the inverse of the source power spectrum) for 2004 and 2005, on the same scale as (a) and (b).

The imprint of varying source power spectrum on the virtual-source data can be removed by deconvolving each trace of the correlation gather by the power spectrum of the corresponding source. This is like applying a filter that represents the inverse of the source power spectrum. We refer to the convolution of the estimated source power spectrum and its designed inverse as *self-decon*. Ideally, the self-decon for both 2004 and 2005 should be the same band-limited delta function. Any variation in the source power spectrum for 2004 and 2005 should be suppressed in the difference of the self-decons.

The difference in the self-decons is displayed in Figure 8d. The deconvolution operators for 2004 and 2005 were the same. But because the operation was applied to a windowed direct arrival in the autocorrelation gather, early time reflections and refracted arrivals contaminated the direct arrival, causing the self-decons to be different. The interference of early time reflections and refracted arrivals shows up as the curved events in Figure 8d. Apart from the curved events representing the interference of other events with the direct arrival, the systematic residual bubble variation is suppressed. Thus, deconvolving the correlation gather with the estimated source power spectrum successfully suppresses the source power spectrum variations. In the consecutive virtual-source images, we apply the designed inverse filters to the correlation gathers to suppress the variations in the source signature (residual bubble).

Therefore, a better way to generate virtual-source data is to correlate the downgoing waves at the virtual source with the upgoing waves at the receivers, followed by deconvolving the correlation gather by the source power spectrum and then summing the correla-

tion gather over the physical sources. Migrating the virtual-source data for 2004 and 2005, generated after applying up-down wavefield separation and deconvolution of the correlation gather by the source power spectrum, results in Figure 9a and b, respectively. The reservoir layers highlighted by the ellipse are well imaged.

Figure 9c is the normalized difference of the images for 2004 and 2005. The improvement in the repeatability by combining up-down wavefield separation and deconvolution of the correlation gather with the autocorrelation of the source-time function is evident by the decrease in the nrms to 16%. As shown in Table 1, time-lapse variations from the source location, seawater, and source signature are suppressed by incorporating up-down wavefield separation and deconvolution by the source power spectrum, respectively, into the virtual-source method. We use all of the downgoing waves at the virtual source for correlation, so variations in the shear waves still exist.

The repeatability can be further improved to suppress the variations in the shear waves by combining up-down wavefield separation, windowing of the direct arrival, and self-decon. The images in Figure 10a and b are obtained by migrating the virtual-source data generated in this way. The reservoir layers highlighted by the ellipse are well imaged. A gap in both images around receiver 80 is a result of the presence of the production platform.

Figure 10c is the normalized difference of the images for 2004 and 2005. The corresponding nrms, after combining up-down wavefield separation, windowing the direct arrival, and deconvolution, reduces from 16% to 14%. As indicated in the last row of Table 1, by com-

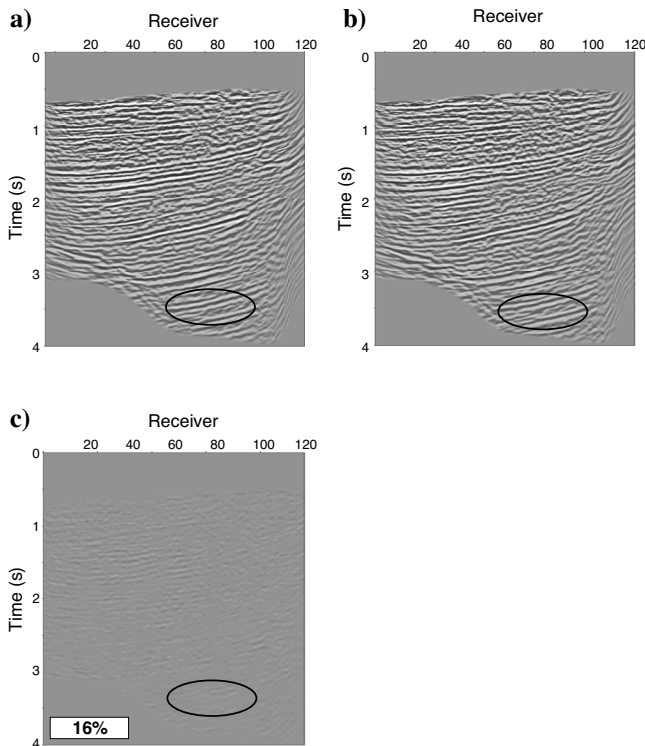


Figure 9. Images generated by migrating the virtual-source data. Virtual-source gathers are generated by correlating the downgoing waves at the virtual source with the upgoing waves at the receivers, followed by deconvolving the source power spectrum before summation. (a) Image for 2004 data. (b) Image for 2005 data. (c) Normalized difference of the two images, after local time alignment, showing the nrms value in the box.

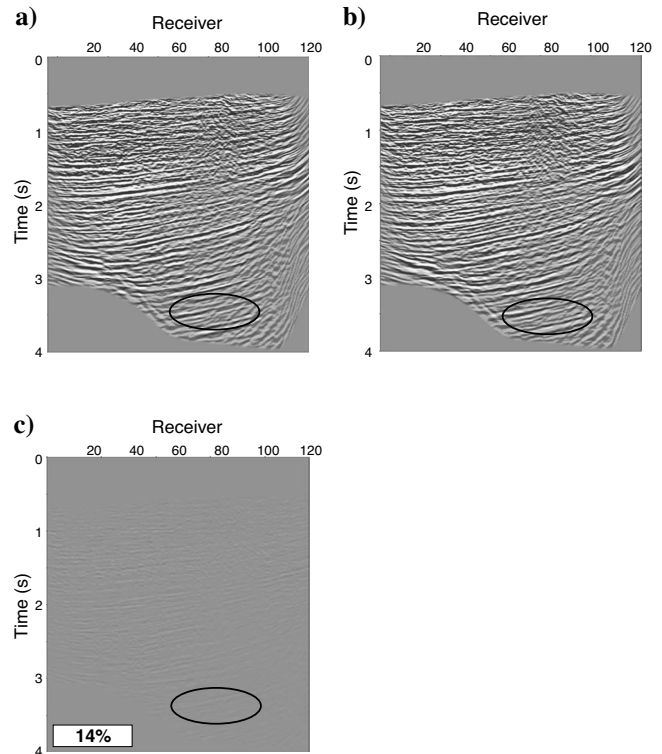


Figure 10. Images generated by migrating the virtual-source data. Virtual-source gathers are generated by correlating the direct arrival windowed in the downgoing waves at the virtual source with the upgoing waves at the receivers, followed by deconvolving the source power spectrum before summation. (a) Image for 2004 data. (b) Image for 2005 data. (c) Normalized difference of the two images, after local time alignment, showing the nrms value.

binning up-down wavefield separation, time-windowing the direct arrival, and applying deconvolution, we can suppress the influence of variations in the seawater as well as acquisition discrepancies (source location and source signature), strengthening the virtual-source method for time-lapse monitoring. However, the reflections and multiples that are downgoing at the virtual source, upgoing at the receivers, and propagating through the time-varying water layer (dashed rays in Figure 5c) still exist.

CONCLUSIONS

A combination of up-down wavefield separation, time-windowing the direct arrival, and deconvolution enhances the repeatability of the virtual-source images, thus strengthening the virtual-source method for time-lapse monitoring. Crosscorrelating the downgoing waves at the virtual source with the upgoing waves at the receivers reduces the influence of the time-varying seawater on the time-lapse virtual-source data. Windowing the direct arrival in the downgoing waves imposes a P-wave virtual source and hence eliminates the temporal variations in the downgoing shear waves. Finally, deconvolution of the correlation gather by the source power spectrum suppresses the lack of repeatability that results from variations in the source power spectrum. Time-lapse monitoring can thus be strengthened by incorporating up-down wavefield separation and deconvolution into the virtual-source method.

ACKNOWLEDGMENTS

We thank Shell for permission to show the Mars OBC data and for financial support through the GameChanger Program. We appreciate the critical comments from David Lumley and anonymous reviewers who helped refine the manuscript.

REFERENCES

- Bakulin, A., and R. Calvert, 2004, Virtual source: New method for imaging and 4D below complex overburden: 74th Annual International Meeting, SEG, Expanded Abstracts, 2477–2480.
- , 2005, Virtual shear source: A new method for shear-wave seismic surveys: 75th Annual International Meeting, SEG, Expanded Abstracts, 2633–2636.
- , 2006, The virtual source method: Theory and case study: *Geophysics*, **71**, no. 4, S1139–S1150.
- Calvert, R., 2005, Insights and methods for 4D reservoir monitoring: Distinguished Instructor Short Course (DISC) manual, 52–58.
- Claerbout, J. F., 1968, Synthesis of a layered medium from its acoustic transmission response: *Geophysics*, **33**, 264–269.
- Curtis, A., P. Gerstoft, H. Sato, R. Snieder, and K. Wapenaar, 2006, Seismic interferometry — Turning noise into signal: *The Leading Edge*, **25**, 1082–1092.
- Derode, A., E. Lacrose, M. Campillo, and M. Fink, 2003, How to estimate the Green's function for a heterogeneous medium between two passive sensors? Application to acoustic waves: *Applied Physics Letters*, **83**, 3054–3056.
- Korneev, V., and A. Bakulin, 2006, On the fundamentals of the virtual source method: *Geophysics*, **71**, no. 3, A13–A17.
- Koster, K., P. Gabriels, M. Hartung, J. Verbeek, G. Deinum, and R. Staples, 2000, Time-lapse seismic surveys in the North Sea and their business impact: *The Leading Edge*, **19**, 286–293.
- Kragh, E., and P. Christie, 2002, Seismic repeatability, normalized rms, and predictability: *The Leading Edge*, **21**, 640–647.
- Larose, E., L. Margerin, A. Derode, B. van Tiggelen, M. Campillo, N. Shapiro, A. Paul, L. Stehly, and M. Tanter, 2006, Correlation of random wavefields: An interdisciplinary review: *Geophysics*, **71**, no. 4, S111–S121.
- Lumley, D., 2001, Time-lapse seismic reservoir monitoring: *Geophysics*, **66**, 50–53.
- Mehta, K., A. Bakulin, J. Sheiman, R. Calvert, and R. Snieder, 2007b, Improving virtual source method by wavefield separation: *Geophysics*, **72**, no. 4, V79–V86.
- , 2007c, Removing artifacts and overburden multiples from virtual source data: 69th Annual Conference and Exhibition, EAGE, Extended Abstracts, E043.
- Mehta, K., J. Sheiman, R. Snieder, and R. Calvert, 2007a, The virtual-source method applied to the Mars field OBC data for time-lapse monitoring: 77th Annual International Meeting, SEG, Expanded Abstracts, 2914–2918.
- Mehta, K., R. Snieder, R. Calvert, and J. Sheiman, 2006, Virtual source gathers and attenuation of free-surface multiples using OBC data: Implementation issues and a case study: 76th Annual International Meeting, SEG, Expanded Abstracts, 2669–2673.
- Naess, O., 2006, Repeatability and 4D seismic acquisition: 76th Annual International Meeting, SEG, Expanded Abstracts, 3300–3303.
- Rickett, J., and J. Claerbout, 1999, Acoustic daylight imaging via spectral factorization: *Heliogeology and reservoir monitoring: The Leading Edge*, **18**, 957–960.
- Robinson, E. A., 1999, *Seismic inversion and deconvolution. Part B: Dual-sensor technology*: Pergamon-Elsevier.
- Schuster, G. T., J. Yu, J. Sheng, and J. Rickett, 2004, Interferometric/daylight seismic imaging: *Geophysical Journal International*, **157**, 838–852.
- Snieder, R., 2004, Extracting the Green's function from the correlation of coda waves: A derivation based on stationary phase: *Physical Review E*, **69**, 046610.
- Snieder, R., J. Sheiman, and R. Calvert, 2006a, Equivalence of the virtual source method and wavefield deconvolution in seismic interferometry: *Physical Review E*, **73**, 066620.
- Snieder, R., K. Wapenaar, and K. Larner, 2006b, Spurious multiples in interferometric imaging of primaries: *Geophysics*, **71**, no. 4, S165–S178.
- Wapenaar, K., 2004, Retrieving the elastodynamic Green's function of an arbitrary inhomogeneous medium by crosscorrelation: *Physical Review Letters*, **93**, 254301.
- Wapenaar, K., J. Fokkema, and R. Snieder, 2005, Retrieving the Green's function by crosscorrelation: A comparison of approaches: *Journal of the Acoustical Society of America*, **118**, 2783–2786.